IIETA International Information and Engineering Technology Association
Advancing the World of Information and Engineering

Journal of New Materials for Electrochemical Systems
Vol. 26, No.3, July 2023, pp.206-214
Journal homepage: http://iieta.org/journals/jnmes

Natural Zeolite-Cellulose Phosphate Nanocomposites: Preparation and Advance Electrochemical Study

Ivelina Tsacheva [1,*], Mariela Dimitrova [2], Adriana Gigova [2], Ognian Dimitrov [2], Dzhamal Uzun [2,*]

[1] Institute of Polymers, Bulgarian Academy of Sciences, Acad. G. Bonchev Street, Sofia, 1113, Bulgaria
[2] Institute of Electrochemistry and Energy Systems "Academician Evgeni Budevski", Bulgarian Academy of Sciences, Acad. G. Bonchev Street., Sofia, 1113, Bulgaria

Corresponding Authors Email: itsacheva@polymer.bas.bg; dzhamal.uzun@iees.bas.bg

https://doi.org/10.14447/jnmes.v26i3.a08

Received: April 7-2023
Accepted: August 9-2023

Keywords:
cellulose phosphate, electrocatalyst, microwave irradiation, nanocomposites, natural zeolite, purification of organic pollutants, seawater electrolysis

ABSTRACT

The scope of this research study is to investigated the green method for preparing and applying cost-effective and environmentally friendly electrocatalytic materials from natural zeolite (clinoptilolite) and cellulose phosphate using microwave irradiation. X-ray diffraction (XRD), scanning electron microscopy (SEM), energy-dispersive spectroscopy (EDX) and Brunauer-Emmett-Teller (BET), were used for the physicochemical characterization of nanocomposites. The newly obtained nanocomposites were studied electrochemically using cyclic voltammetry, linear sweep, galvanostatic measurements, and Tafel slopes.

The results show that the obtained nanocomposites can find applications as promising electrocatalytic materials for seawater electrolysis for hydrogen production at oxygen evolution reactions (OER) and for electrochemical purification of organic pollutants.

NOMENCLATURE

ACPh	alkali Cellulose phosphate
BET	Brunauer-Emmett-Teller
CPh	cellulose phosphate
CV	cyclic voltammetry
DI	deionized water
EDX	energy-dispersive spectroscopy
H^+-NZ	protonated natural zeolite
IR	infrared
MW	microwave
NZ	natural zeolite (clinoptilolite)
OER	oxygen evolution reaction
RHE	reversible hydrogen electrode
SEM	scanning electron microscope
TV35	Teflonized Vulcan XC-72R (35% PTFE)
XRD	X-ray powder diffractometer
ZACPh	nanocomposite from zeolite and alkali cellulose phosphate
ZCPh	nanocomposite from zeolite and cellulose phosphate
ZMEs	zeolite modified electrodes

Greek symbols

j_0	exchange current-density values
η	overpotential
σ	conductivity value

1. INTRODUCTION

Seawater is an inexhaustible resource on the planet, and the production of hydrogen by electrolysis of seawater can be an unavoidable factor in alleviating the energy crisis at ever-increasing demand for energy [1].

Seawater electrolysis has become increasingly attractive for hydrogen production (clean energy), which would produce not only ample surplus renewable electricity but also plentiful freshwater. As one of the most abundant resources on the Earth, seawater is not only a promising electrolyte for industrial hydrogen production through electrolysis but also of great significance for the refining of edible salt. Despite the great potential for large-scale hydrogen production, the implementation of water electrolysis requires efficient and stable electrocatalysts that can maintain high activity for water splitting without chloride corrosion [2].

Developing stable electrocatalysts for seawater electrolysis is challenging due to the presence of various organic pollutants [3]. The transition metal is a suitable candidate for electrocatalytic water oxidation. Still, corrosion of catalysts and comprise side reactions from industrial pollutants create conditions and ambition in studies of novel electrocatalysts materials [4]. Looking of efficient electrocatalytic materials is the key to reducing overpotential Oxygen Evolution Reaction (OER) in alkaline solution [5].

A zeolite material as natural and synthetic crystalline aluminosilicates offer many unique and specific chemical, physical, and structural properties. Zeolite modified electrodes (ZMEs) have been widely studied in the last decades, and many reviews concerning modification of the electrode surface with zeolites, including methods of their

preparation, mechanism of charge transfer, and analytical application of ZMEs have appeared in the literature [6-7]. The growing interest in the use of ZMEs for electroanalytical purposes results from the specific framework structure of zeolites containing the three-dimensional system of cages and channels with various shapes, sizes, and topologies, which determine their molecular sieve properties, as well as the ability to undergo the ion-exchange process with transition metals, resulting in their catalytic property. Additionally, stability in high temperatures, insolubility in most organic solvents, and resistance in acid media make zeolites an attractive modifying agent [8-10].

Natural zeolites (NZ) are crystalline hydrated aluminosilicate minerals with numerous pores filled with alkali, alkaline earth cations, and water and possess valuable physicochemical properties such as unique selective sorption, ion exchange, and thermal stability [11].

Carlos et al. found that ultrasonic pretreatment has an important effect on the reduction processes and on the morphology of the electrodeposited sample [12].

Traditionally, organic synthesis is carried out by conductive heating with an external heat source (for example, an oil bath). This is a comparatively slow and inefficient method for transferring energy into the system since it depends on the thermal conductivity of the various materials that must be penetrated, and results in the temperature of the reaction vessel being higher than that of the reaction mixture. In contrast, microwave irradiation produces efficient internal heating (in-core volumetric heating) by direct coupling of microwave energy with the molecules (solvents, reagents, catalysts) that are present in the reaction mixture. Since the reaction vessels are typically made out of (nearly) microwave-transparent materials, such as borosilicate glass, quartz, or Teflon, an inverted temperature gradient results compared to conventional thermal heating [13].

Microwave (MW) possesses not only instantaneous heating and hot spot effect but also a high catalytic effect. Meanwhile, the MW irradiation technique has been chosen since it produces thin films for a short duration at low temperatures, and the monomer conversion is increased, the side reaction is reduced, and thus the purity and yield of obtained material are further improved [14-15].

Kandasamy et al. have been studied the MW treatment of graphene/polyaniline nanocomposite to improve the porous nature and electronic conductivity. They found that MW treatment of the composite is important for the high electrochemical performance of the electrodes and improves the porous nature of the composite, which further improves the charge transfer mechanism and ion transport through the electrodes [16].

Meena et al. described properties of biopolymer magnetic nanocomposites for various applications as well as adsorptions of inorganic metal, organic pollutants, bio-sensing, catalysis activity, energy, environmental remediation, wastewater treatment and textiles, etc. [17].

Cellulose-based materials also show interesting electrical properties. For example, alkali-cellulose conductivity measurements of polyethylene oxide/carboxymethyl cellulose blends have revealed with 30/70 wt.%, an electrical conductivity of 5.19 ×10-5 $S.cm^{-1}$ has been achieved [18-20]. Furthermore, alkali-cellulose ($C_6H_{10}O_5$* NaOH) prepared by treatment of cellulose fibers with an aqueous solution of sodium hydroxide (mercerization) yielded an increase in the interchains distance of cellulose due to the breakage of some intermolecular hydrogen bonds [21-23]. Ethylcellulose exhibits preeminent film-forming and mechanical properties, and the incorporation of the phosphates of Ni (II), Sn, or Mg (II) in its structure enhances electrochemical conductivity [24]. The effects of inserting sodium cation by mercerization of cellulose on the crystalline structure and electrical conductivity of cellulose are significant. Indeed, alkali cellulose has been classified as a fast-ionic conductor with a conductivity value of $\sigma 473\ K = 3.22 \times 10\text{-}6\ S.cm^{-1}$ and activation energy of Ea1 (393-458K) = 0.49 eV and Ea2 (459-500K) = 0.68 eV [25]. These electrochemical performances can be exploited for advanced applications related to biosensors and pharmaceutical products [24-26].

Recently was reported that cellulose particles were used as an effective approach for removing environmental contamination (methylene blue) caused by textile industry waste. Because of its ability to remove cationic dyes, the cellulose derived from sugarcane bagasse is a particularly beneficial product for the environment. Cellulose particles have a high maximum adsorption capacity of methylene blue (66.386 mg/g). The high maximum adsorption capacity achieved on sugarcane bagasse-derived cellulose is evidence that it can be used to treat textile industry waste containing cationic dyes [27].

P-doped materials are with good catalytic efficiency and recyclability combined with a rapid, energy-saving approach that permits fabrication on a large scale [28].

P-doped porous materials are promising materials for "green catalysis" due to their higher theoretical surface area, sustainability, environmental friendliness, and low cost [29].

The main focus of this work was to study the methods of preparation of nanocomposites from natural zeolite (NZ) and Cellulose phosphate (CPh) or alkali Cellulose phosphate (ACPh) using MW irradiation. Conditions, such as irradiation power and time, required to optimize the preparation of zeolite electrochemical materials were studied. The obtained nanocomposites have been investigated for application in electrochemical processes like purification of organic compounds and electrolysis of seawater for hydrogen production.

This green procedure will open further research directions for the preparation and application of cost-effective and environmentally friendly electrocatalytic materials based on natural zeolite (clinoptilolite) modified with cellulose phosphate for application in different electrochemical systems like green hydrogen production and cleansing of waste water containing organic pollutant.

2. EXPERIMENTAL

2.1. Materials and Methods

Cellulose phosphate (CPh), NaOH, NH_4Cl were purchased from Sigma-Aldrich. Natural zeolite (NZ) – zeolite (clinoptilolite) from the Rhodopes, Bulgaria.

Microwave-assisted reactions were carried out in Microwave Reactor ROTO SYNTH Rotativ Solid Phase purchased from Milestone, Bergamo, Italy.

The newly obtained nanocomposites were analyzed for crystalline phases by X-ray powder diffractometer (XRD) PANalytical Aeris, with CuKα radiation (λ = 1.5406Å) and θ-θ Bragg-Brentano geometry. The scan range size was 5-50° 2θ with 0.02° step size and 60s per step. Diffractograms

interpretation was performed using the database PDF 2 - 2022, ICDD.

The surface morphology of the samples was studied with a scanning electron microscope (SEM) Zeiss Evo 10. The images were taken in high vacuum mode with 25 kV accelerating voltage using secondary electrons signal. The chemical composition of the surface was investigated with a Zeiss SmartEDX microanalysis system with a 30 mm^2 detector active area and 129 eV energy resolution at a take-off angle of 31.5.

The measurements of the sorption isotherms were made on an AutoSorb device - from the company Quantachrome Instrument (USA). The autosorb iQ has the capability of measuring adsorbed or desorbed volumes of nitrogen at relative pressures in the range of 0.001 to slightly less than 1.0. This volume-pressure data can be reduced by the autosorb iQ software into BET surface area, adsorption and/or desorption isotherms, pore size distributions, and total pore volume.

The 1 cm^2 electrodes were studied by, steady-state polarization curves and Tafel analysis. The cell volume was 50 ml. A minimum of three measurements were made for each result to achieve better reproducibility. Arithmetic averages are presented in the graphs. The electrochemical measurements were conducted using "Gamry Interface 1010E".

2.2. Preparation of alkali Cellulose phosphate (ACPh)

An amount of 0.5 g of CPh (Sigma-Aldrich) was immersed for 3 h in 100 ml of an aqueous solution of NaOH (20%) at room temperature. The resultant polymer was recovered by simple filtration (without additional washing) and dried at 50 °C in a vacuum dryer to constant weight. The obtained sample was ($C_6H_{10}O_5O$-$P(ONa)_2$*NaOH) [25].

2.3. Preparation of protonated natural zeolite (H^+-NZ)

To obtain the protonated form of the natural zeolite (H^+-NZ), ion exchange was performed using MW irradiation (similar to the procedure described in [30]). Natural zeolite (0,5 g) and 2 M ammonium chloride (NH_4Cl) (10 ml) were mixed in an open vessel. The reaction was carried out under MW irradiation (200 W) at a hold temperature of 130 °C read by an IR thermometer. The reaction was completed for 30 minutes. The product was washed three times with DI water, recovered by simple filtration and dried at 50 °C under vacuum to constant weight.

2.4. Preparation of nanocomposites from Zeolite and Cellulose phosphate (ZCPh)

To the H+-NZ was added CPh 1:1 (ZCPh-1), 1:2 (ZCPh-2), 1:2.5 (ZCPh-3) by weight and about 10 ml of DI water. The reaction was carried out under MW irradiation at a hold temperature of 110 °C, read by an IR thermometer. The reaction proceeds for 30 minutes at 200 W and 240 minutes at 100 W, respectively (see Table 1). The reaction mixture was washed three times with DI water, recovered by simple filtration and dried at 50 °C under vacuum to constant weight.

2.5. Preparation of nanocomposites from Zeolite and alkali Cellulose phosphate (ZACPh)

CPh (0.5 g) was added to 20% NaOH (100 ml) for 3 hours at room temperature without stirring. The phosphorus content of cellulose is about 12% [26].

After the time has elapsed, the ACPh was filtered by simple filtration and dried at 50 °C under vacuum to constant weight.

To the H^+-NZ was added ACPh 1:1 (ZACPh-1) and 1:2 (ZACPh-2) by weight and about 20 ml of DI water. The reaction was carried out under MW irradiation at a hold temperature of 110 °C, read by an IR thermometer. The reaction was completed for 30 minutes at 200 W. The reaction mixture was washed three times with DI water, recovered by simple filtration and dried at 50 °C under vacuum to constant weight.

2.5. Electrode Preparation

Different sample electrodes of the immersed type were prepared by deposition of the sample catalyst on the work surfaces of all electrodes, followed by pressing and heating [31].

The electrodes studied have geometrical areas of 1 cm^2. The electrodes were prepared from a mixture of the catalyst mass (constant for all electrodes – 100 mg) and Teflonized carbon Vulcan XC-72 (35% Teflon) as a binder content of 50 mg/cm^2. The mixture was pressed onto both sides of a stainless steel current collector at 300 °C.

3. RESULTS AND DISCUSSION

3.1. Reaction conditions

Novel nanocomposites were prepared under MW irradiation: through the addition of NZ to CPh or ACPh in the ratio 1:1 and 1:2 by weight, heating the reaction mixture at 200 W for 30 minutes. Nanocomposites ZCPh-3 and ZCPh-4 were prepared in a ratio of 1:2.5, heating the reaction mixture at 100 W for 180 minutes. For nanocomposite ZCPH-4.1 the ratio was 1:2.5, heating the reaction mixture at 100 W for 240 minutes. Reactions were performed using DI water as a wetting agent.

Table 1. Reaction conditions for the preparation of nanocomposites

Nanocomposites Samples	NZ:CPh, weight	MW, watts	Reaction time, min
NZ	-	-	-
TV35	-	-	-
ZCPh-1	1:1	200	30
ZCPh-2	1:2	200	30
ZCPh-3	1:2.5	100	180
ZCPh-4	1:2.5	100	180
ZCPh-4.1	1:2.5	100	240
ZACPh-1	1:1	200	30
ZACPh-2	1:2	200	30

3.2. XRD Studies

XRD analysis was performed for all obtained nanocomposites. The diffractogram of the used NZ shows a mixture of clinoptilolite and heulandite [K-exchanged], whose main peaks are at 22,37º and 9.86º 2θ, respectively (Figure 1). The obtaining of H^+-NZ has been demonstrated

by a slight shift of the peaks, as well as the increasing intensities of the main ones.

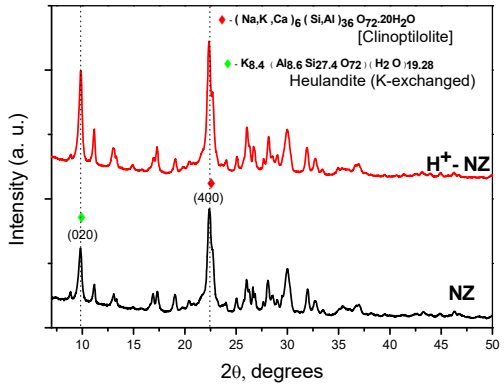

Figure 1. XRD of NZ and H+-NZ

The next figures present the transformation of the H^+-NZ after adding CPh (Figure 2a) and ACPh. (Figure 2b). The absence of a clear diffraction peak between 19°-22.6° 2θ corresponding to the cellulose, as well as the appearance of an amorphous halo, are due to the reduced number of intra-molecular hydrogen bonds as a result of the introduction of phosphate groups in the structure of cellulose [32-33]. The diffractograms of all nanocomposites show that polymerization is also observed in the mechanical mixing of the components. Still, the polymerization processes are complete at MW synthesis and are further favored by introducing more CPh (Figure 2a - NZ:CPh=1:2) or ACPh (Figure 2b – NZ:ACPh=1:2).

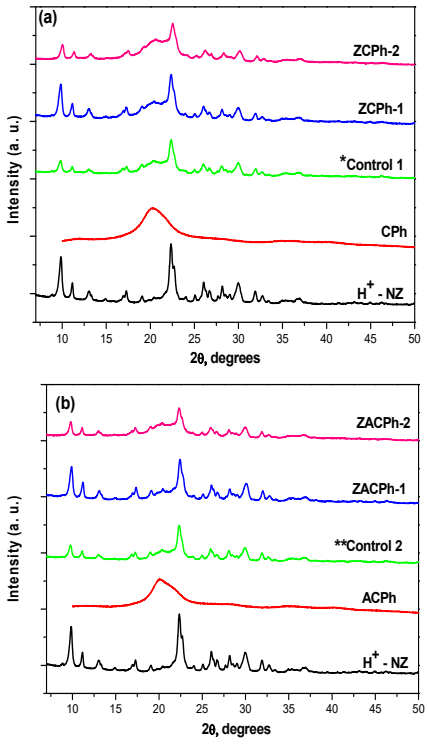

Figure 2. XRD patterns of (a) zeolite nanocomposites with CPh and (b) zeolite nanocomposites with ACPh

The XRD characterizations of obtained zeolite nanocomposites depending on the type of cellulose phosphate (CPh or ACPh) are presented in Figure 3. In the case when the synthesis was carried out with ACPh there are slight changes in the diffraction pattern, which may be associated with implemented Na cation. The peaks appearing in the amorphous halo region correspond to the H^+-NZ, but their sharpening and displacement from 19.74° to 19.81° 2θ also from 20.40° to 20.44° 2θ at impregnation with ACPh can be explained by the formation of a new phase ($Na_3PO_4.8H_2O$), whose main peaks are at 20.44° and 19.81° 2θ (Figure 3a). The same diffraction pattern was observed when the ratio of H^+-NZ:CPh is 1:2 (Figure 3b).

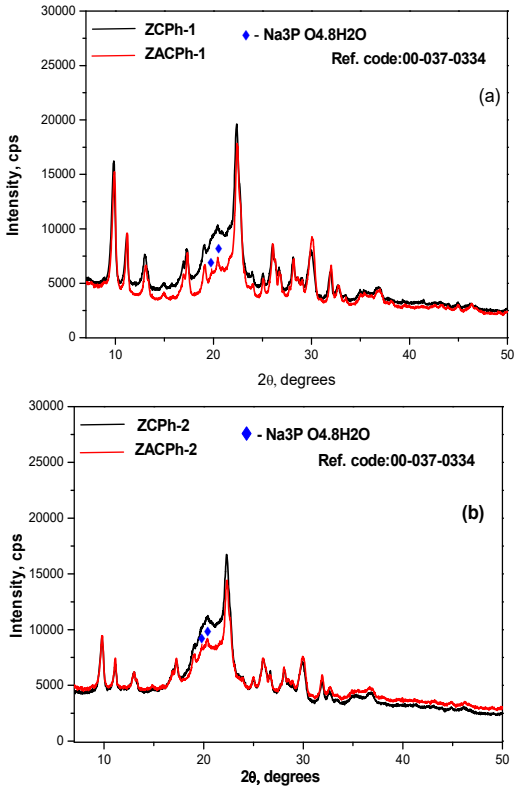

Figure 3. XRD patterns of (a) H^+-NZ:CPh=1:1 and H^+-NZ:ACPh=1:1 and (b) H^+-NZ:CPh=1:2 and H^+-NZ:ACPh=1:2

A comparison of the samples of zeolite modified under one of the same conditions (amount of CPh and time of zeolite protonation) depending on the duration of MW irradiation was carried out. There is an increase in the intensity and area as well as a shift from 22.37˚ to 22.20˚ 2θ of the main peak of clinoptilolite in the sample subjected to longer MW synthesis (sample ZCPh-4.1). An increase in the area of the amorphous halo is also observed. This phenomenon can be explained by the increasing disorder of the zeolite structure [34] and indicates a higher degree of polymerization.

3.3. SEM analysis

The surface morphology of the natural zeolite material (NZ) and the microwave-assisted synthesized nanocomposite ZCPh-4.1 was investigated with scanning electron microscopy. Figure 5 shows SEM micrographs of the natural zeolite material taken at high magnifications.

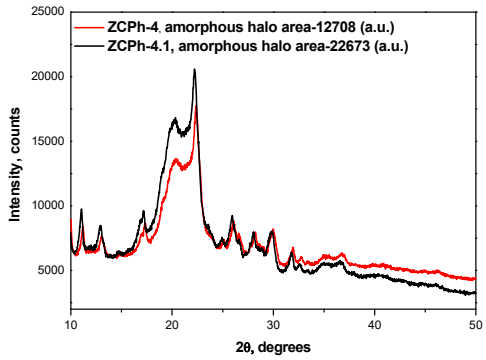

Figure 4. XRD patterns of modified zeolite depending on the duration MW irradiation

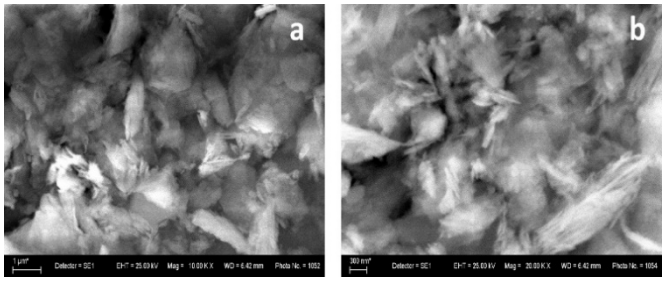

Figure 5. SEM images of the natural zeolite material (NZ) at (a) 10 000 times magnification and (b) 20 000 times magnification

The images reveal that this sample possesses really fine morphology. It consists of variously shaped clusters of fiber-like material with pores forming around these structures. Though the individual clusters are between 300 nm and 1 µm wide, their elongated fiber-like building blocks are much smaller. The image taken at 20 000 times magnification (Figure 5 b) shows their diameter is around 25 nm.

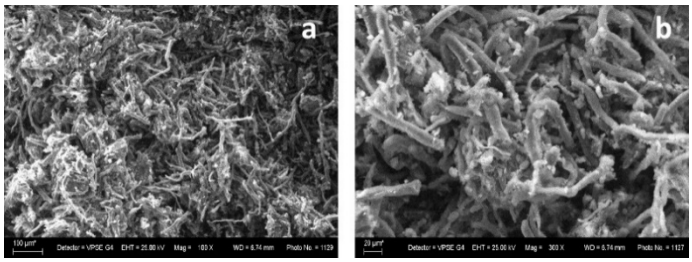

Figure 6. SEM images of the sample ZCPh-4.1 at (a) 100 times magnification and (b) 300 times magnification

Figure 6 shows SEM micrographs of the sample ZCPh-4.1 (the sample with longer MW synthesis) taken at low magnifications. The images reveal that adding cellulose significantly changed the material's microstructure. Large cellulose fibres of around 10 µm in diameter dominate the morphology. They have smaller zeolite clusters attached at their surface and form larger pores between each other as compared with the NZ. A better comparison of the two materials can be seen on Figure 7.

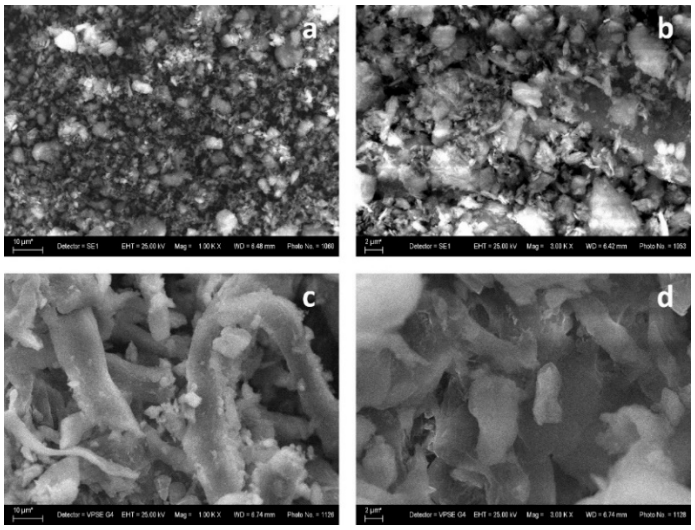

Figure 7. SEM images of sample NZ at magnification of (a) 1000 and (b) 3000 and for sample ZCPh-4.1 at magnification of (c) 1000 and (d) 3000

Figure 7 depicts the stark difference between the NZ and the MW-assisted synthesized nanocomposite ZCPh-4.1. These two materials have very different microstructures, as seen in the images with the same magnification. The NZ is very fine and homogeneous, while the sample ZCPh-4.1 consists of much larger structures thanks to the addition of cellulose.

We have also investigated the chemical composition of these two samples using energy-dispersive spectroscopy, and the results of the EDX analysis are presented in Figure 8.

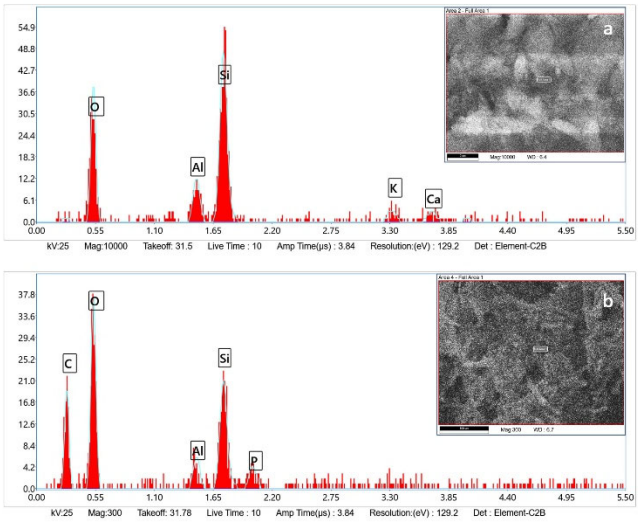

Figure 8. EDX analysis of sample NZ (a) and sample ZCPh-4.1 (b)

The EDX analysis reveals that in addition to the Si, O and Al, the natural zeolite material has small quantities of K and Ca (around 3% each). This is in accordance with the chemical composition of clinoptilolite on record [35]. The spectrum of sample ZCPh-4.1 shows new peaks corresponding to C and P and a higher intensity peak for O, which further confirms the addition of cellulose phosphate to the material.

3.4. BET Surface Area and Pore Size Analysis

By physisorption of nitrogen gas, the adsorption and desorption isotherms of NZ and nanocomposites ZCPh-1, ZACPh-1, ZCPh-4 and ZCPh-4.1 (see Table 1) were measured. The structural characteristics were determined from the adsorption isotherms, which are summarized in Tables 2 and 3. The complete isotherms are presented in Figures 8, 9, and 10.

Nitrogen adsorption/desorption isotherms of NZ, H^+-NZ after the addition of CPh (ZCPh-1) and ACPh (ZACPh-1) are presented in Figure 8.

The measured sorption isotherms approach Type II according to the IUPAC classification, with H3-type hysteresis. The physisorption of most gases on macro porous adsorbents gives reversible isotherms of this type. The shape is the result of unrestricted monolayer-multilayer adsorption up to high p/p_0. Point B – usually corresponds to the completion of monolayer coverage. Point B is less distinctive in this case and indicates a significant overlap of monolayer coverage and the onset of multilayer adsorption. The thickness of the adsorbed multilayer generally appears to increase without limit when $p/p_0 = 1$ [36].

Table 2. Structural parameters of NZ, ZCPh-1 and ZACPh-1

Characteristics	NZ	ZCPh-1	ZACPh-1
Surface Area (BET), m^2/g	38.1	17.2	19.0
Pore Volume, cm^3/g	0.19 *	0.09 **	0.11***
Pore Diameter (BJH Desorption), nm	3.8	3.8	3.8
Average Pore Diameter, (4V/S), nm	20.0	21.0	22.7

* for pores smaller than 400 nm(D)
** for pores smaller than 345nm(D)
*** for pores smaller than 306 nm(D)

The Surface Area is determined by the BET method. Multipoint BET is determined at relative pressure in the range p/p_0=0.05-0.3. The Pore Diameter was calculated by the BJH (Desorption branch) method. The Pore Volume is calculated at a relative pressure close to 1 (p/p_0=0.99). The Average Pore Diameter is calculated assuming that the pores have a cylindrical geometry at p/p_0=0.99.

The measured structural characteristics of the studied zeolite nanocomposites ZCPh-1 and ZACPh-1 are close. Compared to the original NZ, they have about two times lower Surface Area and Pore Volume. While for all three materials, the Average Pore Diameter are close, and the Pore Diameter - calculated from the desorption branch of the isotherm by the BJH method is the same at 3.8 nm.

Pore size distribution is the distribution of pore volume about pore size. In this case, the pore diameter distribution is calculated from the desorption branch of the isotherm by the Barrett, Joyner, Halenda method (BJH method, Desorption). The differential pore diameter distribution curves for NZ, ZCPh-1 and ZACPh-1 are given in Figure 9. A similar distribution of pores in a narrow range is observed for all three nanocomposite materials, and the peak is at 3.8 nm.

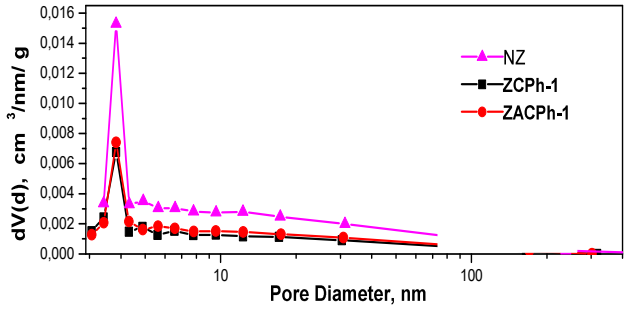

Figure 9. Differential pore diameter distribution curves of NZ, ZCPh-1 and ZACPh-2

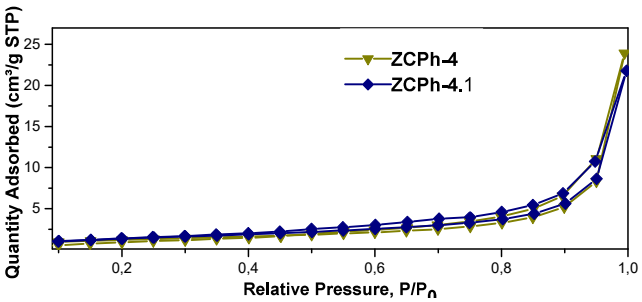

Figure 10. Isotherms of nitrogen adsorption/desorption of modified zeolite with different duration of MW irradiation – ZCPh-4 and ZCPh-4.1

The measured sorption isotherms for ZCPh-4 and ZCPh-4.1 also approach Type II according to the IUPAC classification, but the amount of nitrogen gas adsorbed is significantly less [36].

Table 3. Structural parameters of ZCPh-4 and ZCPH-4.1

Characteristics	ZCPh-4	ZCPh-4.1
Surface Area (BET), m^2/g	4.5	5.2
Pore Volume, cm^3/g	0.037 *	0.034 **
Pore Diameter (BJH Desorption), nm	3.8	3.8
Average Pore Diameter, (4V/S), nm	33.0	26.0

* for pores smaller than 342 nm(D)
** for pores smaller than 400 nm(D)

The measured structural characteristics of ZCPh-4 and ZCPh-4.1 are close. Compared to the original NZ, ZCPh-1 and ZACPh-1 have a significantly lower Surface Area. The measured Pore Volume for pores with a diameter below 342 nm(D) for ZCPh-4 and below 400 nm(D) for ZCPh-4.1 also decreased about 5-6 times compared to the starting NZ and three times compared to ZCPh-1 and ZACPh-1. While the Pore Diameter - calculated from the desorption branch of the isotherm by the BJH method is the same at 3.8 nm, the Average Pore Diameter increases.

3.5. Electrochemical studies

The studies were investigated in three-electrode cell working electrodes (see Table 1), counter electrode platinum

foil, and cell volume 50 cm^2. The used electrolyte is a model solution of seawater 1M KOH + 0.5 NaCl [37].

The newly obtained nanocomposites are studied like electrode materials in electrochemical systems for the oxidation of seawater by different electrochemical techniques: cyclic voltammetry, linear sweep, galvanostatic polarization curves and Tafel analysis.

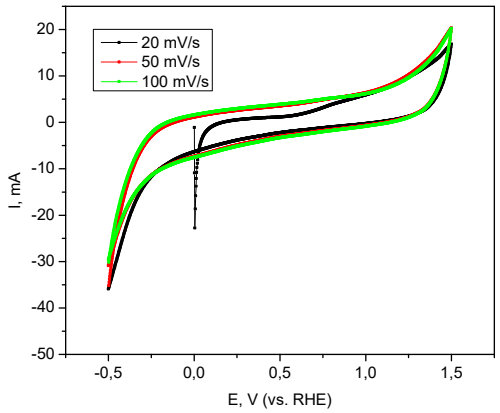

Figure 11. Cyclic voltammetry curves in 1M KOH + 0.5 NaCl, T = 20 °C. Electrodes prepared from ZCPh-4.1. OCP= 671 mV (vs. RHE). Insert presents linearity curve at scan rates 25–100 mV/s

Cyclic voltammetry (CV) was used to investigate the electrochemical behaviour of the ZCPh-4.1 in 1M KOH + 0.5 NaCl. A represents the responses in Figure 11 obtained by CV between -0.6 and 1.6 V (vs. RHE). The ratio between anode and cathode peaks for electrodes at different scan rates demonstrates the reversibility of the system.

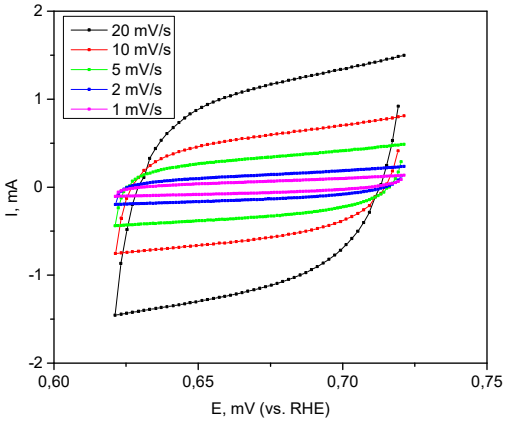

Figure 12. Cyclic voltammetry curves in 1M KOH + 0.5 NaCl, T = 20 °C. Electrodes prepared from ZCPh-4.1. OCP= 671mV (vs. RHE). Insert presents linearity curve at scan rates 1–20 m V/s

A represents the responses in Figure 12 obtained by CV between 0.4 and 0.8 V (vs. RHE). The ratio between anode and cathode parts for electrodes at different scan rates demonstrates similar to conventionally observed capacitive waves.

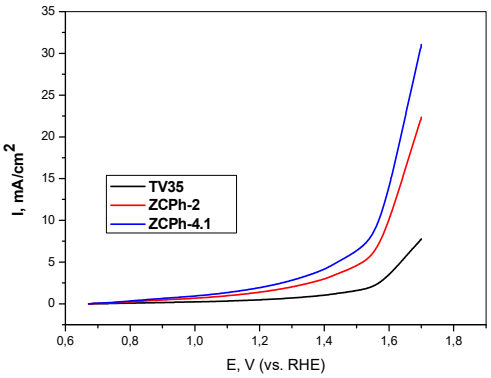

Figure 13. Linear sweep in 1M KOH + 0.5 NaCl, T = 20 °C. Electrodes prepared from ZCPh-4.1; ZCPh-2 and TV35. Open circuit voltage is average between OCP= 655 - 680 mV (vs. RHE)

According to the polarization curves in Figure 13, the ZCPh-4.1 exhibits the highest OER activity with the lowest overpotentials (η) of 899 and 1029 mV to obtain current densities of 10 and 30 mA cm^{-2}. By comparison, 950 mV overpotentials at a current density of 10 mA/cm^{-2} are required for ZCPh-2.

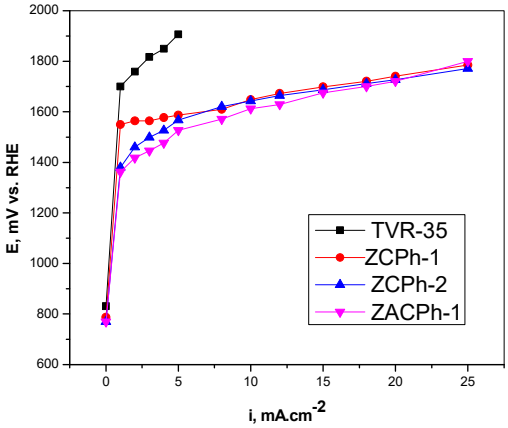

Figure 14. Galvanostatic polarization curves. Electrodes prepared from ZACPh-1 catalysts show good lover overpotential. Electrolyte: 1M KOH + 0.5 NaCl, T = 20 °C

From Figure 14, we observed that electrode prepared from alkali zeolite ZCPh-1 showed good electrochemical characteristics, but it is close to alkalized one. After long-term polarizations, curve analysis observed at studied electrodes without alkali materials works very well.

From Figure 15, we can conclude that the MW process influences the improvement of novel catalytic mass based on zeolite. This can be seen well from the polarization curves.

From initial electrochemical galvanostatic tests, we observed that electrodes with catalytic mass (ZCPh-4.1) obtained after 240 minutes in an MW reactor showed lover overpotential compared with electrodes prepared from pure zeolite and pure Teflonized Vulcan as compartments.

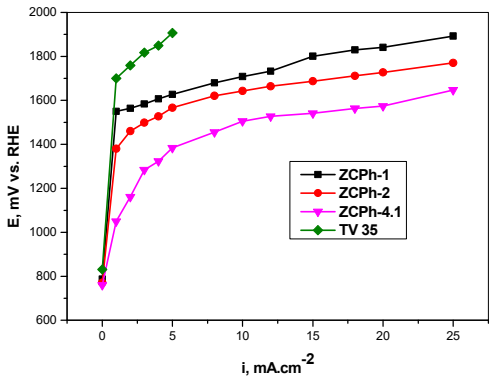

Figure 15. Galvanostatic polarization curves. Electrodes prepared from ZCPh-4.1 catalysts show good lover overpotential compared to literature data. Electrolyte: 1M KOH+0.5 NaCl, T = 20 ºC

From galvanostatic studies, we observed lower overpotential of electrocatalytic materials containing CPh versus ACPh, pure carbon materials and pure NZ. This is probably due to P-doped materials [28-29], although the BET surface area decreases after MW irradiation.

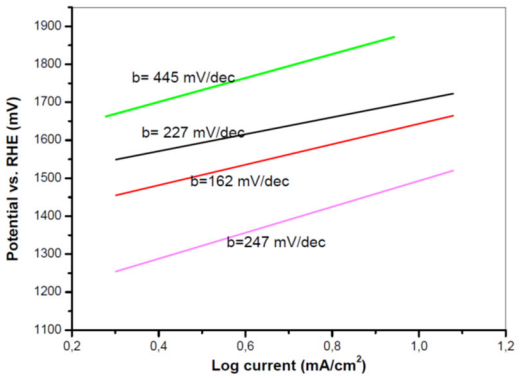

Figure 16. Represents OER and its corresponding Tafel plots of the fabricated electrodes from polarization curves from Figure 15

Our Tafel slopes are not better but are very close and similar to the literature data for non-noble metal-based catalysts for oxygen evolution reactions (OERs) in alkaline media [38]. Tafel slopes of 292, 312 and 393 mV dec−1, in 1.0 M KOH have been describing in the literature electrodes prepared from $NiCo_2O_4$ nanoneedles, CoPi and $NiCo_2O_4$ nanosheets, respectively [39].

In addition, the exchange current-density values (j_0) for the OER are very low beginning from logarithm - 6,17 $mA.cm^{-2}$ for ZCPh's samples were found from Tafel slope extrapolation. The obtained lower oxidation-reduction rate dates at equilibrium j_0 are probably due to front reactions in the study of the electrochemical systems, the nature of materials etc.

4. CONCLUSIONS

In this research study, we propose a green method for the preparation of nanocomposites, from natural zeolite (clinoptilolite) and cellulose phosphate using MW irradiation, as promising electrocatalytic materials. The physicochemical studies (XRD, SEM, EDX and BET) of the obtained new nanocomposites show the successful incorporation of the organic phosphorus compound into the protonated natural zeolite which increases the electrocatalytic properties.

The incorporation of phosphate in zeolite increase the rate of electrochemical processes, that observed with a decrease of overpotential at improved zeolite cellulose phosphate modification.

The resulting zeolite modified electrodes exhibit very good electrochemical properties and lower overpotentials than other studies' electrode samples.

These new materials can find application in the development of design in zeolite modified electrodes improving OER performance with regards to seawater electrolysis, for green hydrogen production and also can find application in purification of organic pollutants.

ACKNOWLEDGMENT

The equipment used at the research are provided by the National Roadmap for Research Infrastructure 2017-2023 “Energy storage and hydrogen energetics (ESHER)”, approved by DCM No 354/29.08.2017 under Grant Agreement DO1-160/28.08.2018.

The authors kindly acknowledge the financial support of the National Science Fund at the Bulgarian Ministry of Education and Science of the project № KP-06-H67/6 – 12.12.2022 – “Bioelectrochemical systems for organic pollutants remediation”.

REFERENCES

[1] Jiang, S., Suo, H., Zhang, T., Liao, C., Wang, Y., Zhao, Q., Lai, W. (2022). Recent Advances in Seawater Electrolysis. Catalysts, 12, 123. https://doi.org/10.3390/catal12020123

[2] Wang, C., Shang, H., Jin, L., Xu, H., & Du, Y. (2021). Advances in hydrogen production from electrocatalytic seawater splitting. Nanoscale, 13(17): 7897-7912.

[3] Malek, A., Lu, X., Shearing, P. R., Brett, D. J. L., He, G. (2022)."Strategic comparison of membrane-assisted and membrane-less water electrolyzers and their potential application in direct seawater splitting (DSS)." Green Energy & Environment, 8(4): 989-1005.

[4] Hui-Min Yang, Zhong-Yong Yuan, (2023). Transition Metal-Based Electrocatalysts for Hydrogen Generation and Related Energy Carrier, ACS Symposium SeriesVol. 1435, Chapter 1: 1-20.

[5] Yadav, Manish Kumar, Chinky Gangwar, and Narendra Kumar Singh. "Low Temperature Synthesis and Characterization of NixFe3-xO4 (0≤ x≤ 1.5) Electrodes for Oxygen Evolution Reaction in Alkaline Medium. (2020) Journal of New Materials for Electrochemical Systems 23.2 (2020): 78-86.

[6] Muresan, L. M. (2010). Zeolite-modified electrodes with analytical applications. Pure and Applied Chemistry, 83(2), 325-343.

[7] Rolison, D. R. (1990). Zeolite-modified electrodes and electrode-modified zeolites. Chemical Reviews, 90(5), 867-878.

[8] Porada, R., Fendrych, K., & Baś, B. (2021). Development of novel Mn-zeolite/graphite modified Screen-printed Carbon Electrode for ultrasensitive and

selective determination of folic acid. Measurement, 179, 109450.

[9] Guzmán-Vargas, A., Oliver-Tolentino, M. A., Lima, E., & Flores-Moreno, J. (2013). Efficient electrocatalytic reduction of nitrite species on zeolite modified electrode with Cu-ZSM-5. Electrochimica Acta, 108, 583-590.

[10] Porada, R., Fendrych, K., & Baś, B. (2020). The Mn-zeolite/Graphite Modified Glassy Carbon Electrode: Fabrication, Characterization and Analytical Applications. Electroanalysis, 32(6): 1208-1219.

[11] Liu, P.; Zhang, A.; Liu, Y.; Liu, Z.; Liu, X.; Yang, L.; Yang, Z. (2022). Adsorption Mechanism of High-Concentration Ammonium by Chinese Natural Zeolite with Experimental Optimization and Theoretical Computation. Water, 14, 2413. https://doi.org/10.3390/w14152413

[12] Carlos, F.S.J., Savadogo, O., Oishi, K., Reyes-Cruz, V.E., Veloz-Rodríguez, M.A. (2016). Electrodeposition of iron from kaolin clay and the effect of mass transport. Journal of New Materials for Electrochemical Systems, 19(2):103-107. https://doi.org/10.14447/jnmes.v19i2.337

[13] Kappe, C. Oliver. (2004). Controlled microwave heating in modern organic synthesis. Angewandte Chemie International Edition 43.46, pp. 6250-6284.

[14] Rahman M.Y.A., Roza L., Samsuri S.A.M., Umar A.A., Salleh M.M. (2017). Dye-sensitized solar cell (DSSC) utilizing TiO2 films prepared via microwave irradiation technique: Effect of TiO2 growth time. Journal of New Materials for Electrochemical Systems, 20(2):59-64. https://doi.org/10.14447/jnmes.v20i

[15] Qu, Jianhua, et al. (2022). Microwave-assisted synthesis of polyethylenimine-grafted nanocellulose with ultra-high adsorption capacity for lead and phosphate scavenging from water. Bioresource Technology 362 127819.

[16] Kandasamy, S.K., Kandasamy, K. (2019). Graphene – polyaniline nanocomposite treated with microwave as a new supercapacitor electrode and its structural, electrochemical properties. Journals of New Materials for Electrochemical Systems, 22(3): 125-131. https://doi.org/10.14447/jnmes.v22i3.a02

[17] Warkar, S.G., Meena, J. (2022). Synthesis and applications of biopolymer /FeO nanocomposites: A review. Journal of New Materials for Electrochemical Systems, 25(1):7-16. https://doi.org/10.14447/jnmes.v25i1.a02

[18] Shakoor RA, Seo DH, Kim H, Park YU, Kim J, Kim SW et al., (2012). J Mater Chem 22:20535–20540.

[19] Tanvir, A.,Chintan, K. (2014). Electrochemistry 6:403–421.

[20] Pu X, Rong C, Tang S, Wang H, Cao S, Ding Y et al., (2019).Chem Commun 55: 9043–9046.

[21] Keshk SMAS, (2015). Carbohydr Polym 115:658–663.

[22] Tsakova V and Seeber R, (2016). Electrochemistry 408:7231–7241.

[23] Mohammad F, Arfin T and Al-Lohedan HA, (2017). Mater Sci Eng C 71:735–743.

[24] Keshk SMAS, Syef AF, El-Zahhar A, Yousef S and Bondok S, (2018). Transylvanian Rev 16:7609–7619.

[25] Marzouki R, Brahmia A, Bondock S, Keshk SMAS, Zid MF, Al-Sehemi, A.G., Koschella, A., Henze, T. (2019). Carbohydr Polym 221:29–36. DOI: 10.1016/j.carbpol.2019.05.083

[26] Marzouki, Riadh, Brahmia, A., Alsulami, Q. A., Keshk, S. MAS, Emwas, A.-H., Jaremko, M., Zid, M. F., Heinze, T. (2021). Structure, thermal stability and electrical properties of cellulose-6-phosphate: development of a novel fast Na-ionic conductor. Polymer International 70. 1290-1297.

[27] Fathana, H., Rahmi, Adlim, M., Lubis, S., Iqhrammullah, M. (2023). Sugarcane bagasse-derived cellulose as an eco-friendly adsorbent for azo dye removal. International Journal of Design & Nature and Ecodynamics, 18(1):11-20. https://doi.org/10.18280/ijdne.180102

[28] Farzinpour, Farzaneh, et al. "Synthesis and study of electrochemical properties of Ni-Co-V@ PrGO to enhance hydrogenevolution reaction." International Journal of Hydrogen Energy 48.55 (2023): 21249-21258.

[29] Patel, Mehulkumar A., et al. "P-doped porous carbon as metal free catalysts for selective aerobic oxidation with an unexpected mechanism." ACS nano 10.2 (2016): 2305-2315.

[30] Jiang, S.; Suo, H.; Zhang, T.; Liao, C.; Wang, Y.; Zhao, Q.; Lai, W. (2022). Recent Advances in Seawater Electrolysis. Catalysts, 12, 123. https://doi.org/10.3390/catal12020123

[31] Idris, A., Saleh, T., Muraza, O., Sanhoob, M., Aziz, M. A., & Al-Betar, A. R. (2019). Synthesis of phosphate-modified zeolite as a modifier in carbon paste electrode for nitrite electrochemical detection. Journal of Materials Science: Materials in Electronics, 30, 3283-3293.

[32] Daud, W. R. W., Kassim, M. H. M., & Mohamded, M. A. S. (2011). Cellulose phosphate from oil palm biomass as potential biomaterials. BioResources, 6(2): 1719-1740.

[33] Gao, C., Xiong, G. Y., Luo, H. L., Ren, K. J., Huang, Y., & Wan, Y. Z. (2010). Dynamic interaction between the growing Ca–P minerals and bacterial cellulose nanofibers during early biomineralization process. Cellulose, 17(2): 365-373.

[34] Pilter, Z., Szabo, S., Hasznos-Nezdei, M., & Pallai-Varsanyi, E. (2000). X-ray diffraction study of the effect of microwave treatment of zeolite Na-A. Microporous and mesoporous materials, 40(1-3): 257-262.

[35] Akdeniz, Y., Ulku, S. (2007). Microwave effect on ion-exchange and structure of clinoptilolite. Journal of Porous Materials, 14: 55–60. https://doi.org/10.1007/s10934-006-9008-z

[36] Thommes, M., Kaneko, K., Neimark, A. V., Oliver, J. P., Reinoso, F. R., Rouquerol, J., Kenneth, S. W. Sing, (2015). Physisorption of gases, with special reference to the evaluation of surface area and pore size distribution (IUPAC Technical Report), Pure and Applied Chemistry, https://doi.org/10.1515/pac-2014-1117

[37] Uzun, D., Razkazova–Velkova, E., Petrov, K., & Beschkov, V. (2016). H2S/O2 fuel cells using hydrogen sulfide from Black Sea waters. Journal of Applied Electrochemistry, 46: 943-949.

[38] Kumar, U.N., Malek, A., Rao, G.R. et al. (2022). Chromium Oxynitride (CrON) Nanoparticles: an Unexplored Electrocatalyst for Oxygen Evolution Reaction. Electrocatalysis 13:62–71. https://doi.org/10.1007/s12678-021-00693-4